Responses of Total Electron Content to Solar Flares over Low and Mid-Latitude Regions during Sun Halo Day

C. Idosa, B. Adhikari and K. Shogile

Responses of Total Electron Content to Solar Flares over Low and Mid-Latitude Regions during Sun Halo Day

C. Idosa[1, *], B. Adhikari[2] and K. Shogile[1]
[1]Department of Physics, Jimma University, Jimma, Ethiopia
[2]Department of Physics, St. Xavier's College, Maitighar, Kathmandu, Nepal
*Corresponding Email: chaleidosa2011@gmail.com

ABSTRACT

The responses of total electron content (TEC) to solar flares over low- and mid-latitude regions during the sun halo days were investigated. The research is based on GPS data obtained from Bangalore (13.02117^oN, 77.57038^oE) on May 24, 2021; Cape Town (-33.918861^oN, 18.423300^oE) on October 26, 2020; and North Dakota (46.55756^oN, -96.472300^oE) on December 27, 2021, during the solar halo days. The results of this study demonstrate that the values of TEC increased at Bangalore and Cape Town stations during solar halo days as compared to other days. However, over the North Dakota station, TEC during the sun halo day was greater than that on the days before and after the halo day from around 19:00 UT to 23:59 UT hours. During the sun halo over Bangalore and Cape Town stations, positive relative changes in TEC prevail, suggesting that the action of the interplanetary electric field, the prompt penetration electric field, and the disturbance dynamo electric field lead to higher TEC values. However, during the sun halo over North Dakota station, negative relative changes in TEC prevail, which might be related to the consequence that low solar activity with no earth's field disturbances (a positive Dst) leads to lower ionospheric TEC values. Stations that have greater relative changes in TEC have shown greater power spectrum and global wave spectrum energy. Cape Town has a greater relative change in TEC, a greater power spectrum, and a larger global wave spectrum than Bangalore and North Dakota stations. The values of TEC over three stations are different due to the latitudinal and longitudinal differences in addition to the universal time effects. Finally, solar flares have a major influence on ionosphere electrodynamics, and the upward drift velocity of ionospheres at the low latitude station is more strongly influenced by solar flares due to the effects of the ExB drifts, which induce TEC disturbances during the halo days over the suggested stations.

Keywords: Ionospheric Total Electron Content, TEC variations, Sun halo, Solar flares, Solar wind parameters.

1. INTRODUCTION

Sun halos are light rings that can encircle the sun or moon. If the clouds are patchy the halo may be incomplete [1-2]. At high enough altitudes in the sky, the water vapour condenses and then freezes into ice crystals. The structure of the crystals causes the light to refract as it passes through the ice crystals, similar to what happens when light goes through a prism [3]. The sun halo is the only one of various optical effects generated by the reflection and refraction of light by ice crystals in the atmosphere [4-5].

Sun dogs form whenever the sun is in the sky, generally less than 45 degrees from the horizon and in the same horizontal plane as the observers. Slight hexagonal ice crystals must also be located in the same plane and parallel to the ground. Sun dogs will develop at roughly 22 degrees distant from the sun if all of the ice crystals are generally flat. They usually appear in pairs, one on each side of the sun,

and are sometimes accompanied by a halo, which is created by sunlight refraction through ice crystals oriented in different directions [6-7]. Colder regions are excellent places to observe sun dogs, although many temperate winters form enough ice crystals to create them. Patient observers can also spot moon dogs when the moon is bright, although they can be very difficult to photograph well without an excellent camera and a tripod. In both cases, look slightly to the left or right of the major light emitting body in the sky for smaller, bright objects that often have long tails facing away from the true moon or sun [8].

Different phenomena that occur as a result of the sun's impacts, such as solar eclipses and space weather alerts, are fascinating and useful in comprehending the characteristics of the lower and upper regions of the atmosphere [9-10]. The Earth's ionosphere is a particularly active portion of the atmosphere that expands and contracts in response to the amount of energy it takes from the Sun [11-12].

Solar flares are accompanied with electromagnetic emission at a variety of wavelengths, ranging from solar radio emission to gamma-ray emission from accelerated particle fluxes and coronal mass ejections. The movement of ionized matter in interplanetary space creates a tremendous shock wave, upsets the geomagnetic field, causes magnetic storms, and has an effect on the status of Earth's atmosphere [13]. The ionospheres characteristics are understandable by using the parameter of ionosphere called Total electron content (TEC) [14]. TEC is an important parameter in mitigating the impacts of ionospheres on radio systems. The propagation of radio links between satellites and the ground, which play critical roles in contemporary communications, navigation, and surveillance technologies, departs from free space circumstances in a variety of ways, with significant ramifications for the service's dependability and accuracy [15].

Over the years several studies on the behaviours of ionosphere due to solar flares, coronal mass ejections, geomagnetic storms and solar eclipses were made over different regions of ionosphere [16-24]. The responses of ionospheric TEC indicate both the positive and negative ionospheric effects as a result of space weather alerts such as solar flares, coronal mass ejections, and geomagnetic storms. The ionospheric TEC, on the other hand, exhibits a negative ionospheric response during the solar eclipse because the eclipse reduces the degree

of ionization [25]. It is currently unknown how ionospheric TEC behaves during the formation of sun halo days.

In this research, the responses of ionospheric TEC to solar flares were studied over low latitude region (Bangalore station) on May 24, 2021, and mid-latitude regions (Cape Town on October 26, 2020, and North Dakota on December 27, 2021) during sun halo days. Over the three sun halo days, the authors examined the responses of ionospheric TEC over low and mid-latitude regions. The authors selected three stations where the sun halo occurred to perform this study. They tried to determine if the space weather alert would cause ionospheric changes in the TEC during the halo's formation. This work has been conducted for the first time as a model, and it will help the scientific and ionospheric communities to understand more about the variations in ionospheric TEC during sun halo days.

2. DATA AND METHODOLOGY

The study depends on GPS data obtained at three stations in Bangalore, North Dakota, and Cape Town on May 24, 2021, December 27, 2021, and October 26, 2020, respectively, during Sun Halo Day. The data were obtained from UNAVCO (University NAVSTAR Consortium) website at the (http://www.unavco.org/data/gps-gnssdata/) dual-frequency GPS devices. The authors obtained the information of sun halos from the given websites over three stations: Bangalore, India on May 24, 2021 (https://ca.finance.yahoo.com/news/theres-a-halo-in-the-sky-today-divine-intervention-or-scientific-phenomenon-075553539.html), North Dakota, American state on December 27, 2021 (https://www.kxnet.com/news/the-day-after-the-snowstorm-sun-dogs-greetnorth-dakotans-at-the-start-of-the-work-week/), and Cape Town, South Africa on October 26, 2020 (https://www.sapeople.com/2020/10/26/what-causes-the-halo-around-the-sun-in-cape-town-today/). The solar flare information for May 24 and December 27, 2021; and October 26, 2020 were obtained from SpaceWeather.com (https://spaceweather.com/archive.php?view=1&day=26&month=10&year=2020). The information of solar flare events during three sun halo days selected for present study 1.

Ionospheric TEC is defined by measuring the carrier phase delays of received signals emitted from satellites orbiting above the ionosphere [26]. It is greatly influenced by solar activity. The ionosphere is a region of the Earth's atmosphere in

which the density of free electrons is high enough to affect radio wave transmission [27]. The GPS data are saved in the RINEX format and processed by the GPS-TEC analysis software [28]. The TEC can be obtained from the pseudo-range (P) and phase observations (ϕ) in dual frequency GPS data as [29].

$$TEC = \frac{1}{40.3}\frac{2(f_1 f_2)^2}{f_1^2 - f_2^2}(P1 - P2) \dots\dots\dots (1)$$

$$TEC = \frac{1}{40.3}\frac{2(f_1 f_2)^2}{f_1^2 - f_2^2}(\phi1 - \phi2) \dots\dots (2)$$

Here, P1 and P2 are pseudo-ranges and ϕ1 and ϕ2 are phases of carriers L1 and L2 respectively. The software algorithm calculates slant TEC (STEC) by using group delay measurements and differential phase advance of the L1 and L2 frequencies, Differential Code Biases (DCBs). The GNSS pseudo-ranges are smoothed by carrier phase levelling to reduce the effect of pseudo-range noise on TEC data. The VTEC is obtained using the relations in electrons/m^2:

$$VTEC = STEC X Cos(\chi) \dots\dots (3)$$

Where the zenith angle χ is expressed as

$$\chi = \arcsin\left(\frac{R_E Cos\alpha}{R_E + h}\right) \dots\dots (4)$$

Where α is the elevation angle of the satellite, RE is the mean radius of the Earth, and h is the height of the ionospheric layer, which is assumed to be 400 km.

The Operating Mission as Nodes on the Internet website (OMNIweb) system data sets from (https://omniweb.gsfc.nasa.gov/) were also used to get the values of the solar wind parameters. The change in TEC is calculated to understand the variations of the ionosphere to positive ionospheric effects (enhancement of TEC) and negative ionospheric effects (depletions of TEC) over all sites. Using the observational data from three stations, the change in TEC during the three sun halo days is computed using Equation 5.

$$\Delta TEC = TEC_s - TEC_q \dots\dots (5)$$

Where TECs is TEC during the sun halo day, TECq is TEC value before and after the sun halo day (normal days). Also in order to quantify the TEC enhancements, the relative TEC change (rTEC) were derived from the hourly TEC data as shown in Equation 6:

$$rTEC = \frac{TEC_s - TEC_m}{TEC_m} X 100\% \dots\dots (6)$$

Where TEC_s is the observed TEC value during sun halo day and TEC_m is the 13 day TEC running median. Also, to understand the TEC uncertainty the following Equation 7 is used in this study for all three stations.

$$\sigma TEC = \frac{\sqrt{(TEC_i - \mu)^2}}{N} \dots\dots (7)$$

Where TEC_i is the observed TEC value before, during and after the sun halo days and μ is their running mean, and N is the total number of measurement over all three stations.

In this study, we employed continuous wavelet transforms to understand the behaviour and distribution of the total electron content of solar flares over low- and mid-latitude regions in the solar halo at various scales [30]. Continuous wavelet transforms are powerful tools that provide unbiased true periodicity estimates when the original signal is decomposed into multiples. A detailed description of the continuous wavelet transform can be found in various research papers [31-32]. Using the continuous wavelet transform, we used the formula 6 to compare the power spectra of the three stations before, during and after the solar halo day, respectively. The information of all stations is given in Table 1.

Table 1: Stations information.

Stations	Geogra. Lat.	Geogra. Long.	Geomag. Lat.	Geomag. Long.	Local Time
Bangalore	13.02117°N	77.57038°E	4.761126°N	149.593709°E	UT+5
North Dakota	46.55756°N	-6.472300°E	57.445125°N	-1.327707°E	UT-6
Cape Town	-33.918861°N	18.423300°E	-41.674146°N	80.906946°E	UT+1

Table 2: Solar flare events during three solar flare and sun halo days selected for present study.

Date	Flare Class	Start Time (UT)	Max. peak Time (UT)	End Time (UT)
23 May, 2021	B1.4	00:14	00:21	00:23
24 May 2021	C1	04:46	04:51	04:55
	C2.7	04:59	05:10	05:20
	C2.4	09:09	09:22	09:35
	C2.2	17:00	17:05	17:10
	M1.2	11:00	11:08	11:14
25 May 2021	B1.4	00:14	00:21	00:23
26 December 2021	C1.8	00:12	00:21	00:30
	C2.7	00:33	00:36	00:41
	C1.9	01:26	01:35	01:50
	C2	04:32	04:42	04:49
	C1	18:26	18:32	18:40
	C1.4	18:46	18:59	19:10
	C3.3	20:00	20:12	20:20
27 December 2021	C1.1	23:57	00:02	00:09
	C1	00:27	00:34	00:38
	C1.4	02:16	02:27	02:34
	C1.2	02:53	03:05	03:16
	C1.4	04:06	04:20	04:33
	C1	06:09	06:17	06:25
	C1.3	09:45	09:53	09:59
	C1.4	19:37	19:48	20:00
	C2.2	23:28	23:35	23:42
28 December 2021	M1.89	03:50	04:01	04:10
	M1.6	15:59	16:11	16:20
25 October 2020	B1.8	11:18	11:22	11:26
26 October 2020	B1.7	23:31	23:36	23:40
27 October 2020	C4.3	06:11	06:16	06:21
	C1.4	09:47	09:52	09:56

3. RESULTS AND DISCUSSIONS

The diurnal variations, change in TEC, relative change in TEC, power and global wavelet spectrum, TEC uncertainty, and the variations of the solar wind parameters throughout low and middle latitude regions are validated in this paper using TEC data obtained from three sites: Bangalore, North Dakota, and Cape Town during the sun halo days during normal geomagnetic conditions.

3.1. Diurnal Variations of TEC during the Sun halo days on May 24, 2021, December 27, 2021 and October 26, 2020

Figure 1 depicts the diurnal variability of ionospheric total electron content over Bangalore on May 24, 2021, North Dakota on December 27, 2021, and Cape Town, South Africa, on October 26, 2020.

Over Bangalore, North Dakota, and Cape Town, the observed sun halo describes the ionospheric

features using the parameters called TEC. At Bangalore station, the sun halo is seen around 11:00 AM and lasts for over an hour on May 24, 2021. At North Dakota station, the sun halo was also seen around 11:03 a.m. EST and lasted for an hour on December 27, 2021. Similarly, over Cape Town station, the sun halo was seen at midday and had an unusual ring around the sun.
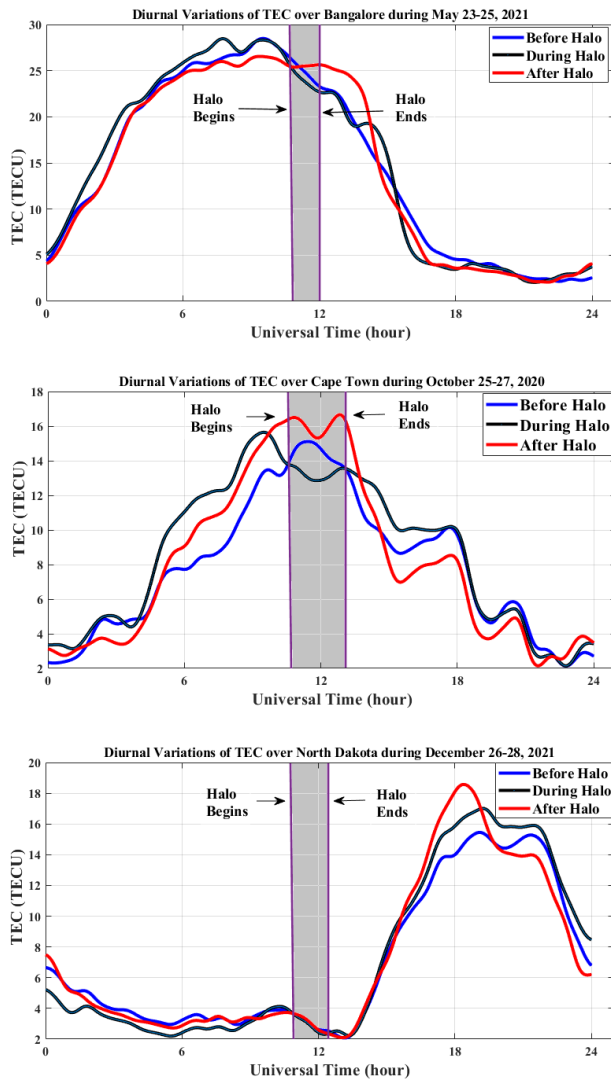
Fig. 1: Diurnal variations of TEC over Bangalore, Cape Town, and North Dakota before, during and after the sun halo days. The blue line is a day before sun halo, black line is during the sun halo and the red one is a day after the halo.

On May 23, 2021, a B1.47 background solar flux with an M1.19 maximum flux was observed. On May 24-25, 2021, the A7.09 background solar flux with a B4.8 maximum flux was observed with a 29 SFU sunspot number. Similarly, on December 26, 2021, the B6.76 background solar flux with a C3.29

maximum flux was observed with a 95 SFU sunspot number. On December 27, 2021, the B4.75 background solar flux and C2.27 maximum solar flux were observed with a 85 SFU sunspot number. On December 28, 2021, the B5.23 background solar flux with the M1.89 maximum flux was observed with a 107 SFU sunspot number. Also, on October 25, 2020, the A1.75 background solar flux with a B1.85 maximum flux was observed. On October 26, 2020, a C4.39 maximum flux was observed with a 22 SFU sunspot number (https://www.spaceweatherlive.com/en/archive/2021/05/24/xray.html).

Over Bangalore and Cape Town stations, TEC during the sun halo day exceeds TEC before and after the sun halo day between 00:00 UT and 09:00 UT. However, during the time when a sun halo is observed, TEC before and after the sun halo exceeds TEC during the sun halo day. Between 00:00 UT (05:00 LT) and 09:00 UT, the value of TEC during the solar halo day exceeds the value of TEC before and after the halo day over Bangalore station (15:00 LT). However, the value of TEC during the halo increased more between 02:00 UT (7:00 LT) and 05:00 UT (10:00 LT). A sun halo occurs when the sun's activity is low, often early in the morning or late at night. Also, TEC during the halo day exceeded A2.28 background solar flux with a B2.31 maximum flux, which was observed with a 17 SFU sunspot number.

However, on October 27, 2020, the B1.39 background solar TEC before and after the halo day over Cape Town will be between 00:00 UT (01:00 LT) and 04:00 UT (5:00 LT). The value of TEC during the halo increased more between 05:00 UT (6:00 LT) and 09:00 UT (10:00 LT). The ionospheric properties over North Dakota, on the other hand, indicate the opposite tendency as those over Bangalore and Cape Town stations. The value of TEC during the December 27, 2021 halo reveals a drop in TEC over North Dakota, particularly between 00:00 UT (17:00 LT) and 19:00 UT (12:00 LT).

3.2. Change in Ionospheric Total Electron Content during the Sun Halo days
We subtract the mean values of the normal days (days before and after the sun halo days) from the TEC values during the sun halo day over each station to comprehend the positive ionospheric total electron content enhancement and the declines in ionospheric total electron content. A comparison of the variations in TEC during normal days and sun halo days is shown in Figure 2. The usual days are the day before the halo and the day after the halo,

15

and ΔTEC is shown across all three stations using Equation 2.

The enhancement of the TEC value was noticed more on the halo day than on other typical days over Bangalore station from 00:00 UT to 10:00 UT. However, between 10:00 UT and 15:00 UT, as well as 16:00 UT and 18:30 UT, TEC was higher on normal days than on halo days.
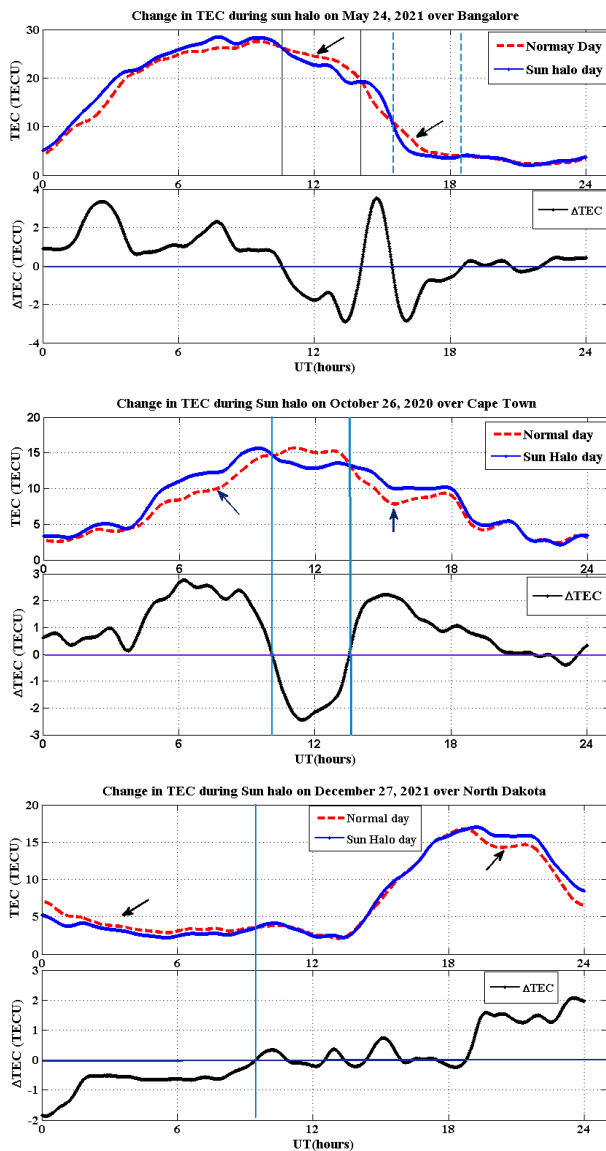
Fig. 2: Variations of change TEC over Bangalore, North Dakota and Cape Town during the sun halo days. The blue line indicates sun halo day, the red one is a normal day, and black line is their differences.

Over Bangalore, TEC was higher on halo days than on other days, indicating that the halo, which is a daytime aurora, may cause a higher ionospheric TEC than on other days. Similarly, during the morning hours of the TEC day, a significant

enhancement was seen over Cape Town station. However, about 13:00 UT (18:00 LT) and 11:30 UT (12:30 LT), respectively, a fall in ionospheric TEC was observed over both Bangalore and Cape Town stations during the sun halo day. The increase in TEC over North Dakota indicates the opposite. Ionospheric TEC increased over Bangalore and Cape Town during this period but decreased over North Dakota. This might be due to the combined effect of the global time difference and local heating conditions. The probable cause of the enhancement of TEC over Bangalore, Cape Town, and North Dakota stations during the sun halo days on May 24, 2021, October 26, 2020, and December 27, 2021, is the two classes of solar flares: C and M classes on May 24, 2021; C-4 class solar flares on October 26, 2020; and C-8 and M-2 class solar flares. TEC is enhanced by solar flares, which are electromagnetic radiation that may enhance the degree of ionization through an enhancement of TEC.

3.3. Relative change in Total Electron Content (rTEC) and Continuous wavelet Transform

Figure 3 shows the relative changes in TEC during the normal days and the sun halo day, and the continuous wavelet transform over Bangalore, Cape Town, and North Dakota stations is plotted, respectively. At around 16:00 UT, the value of rTEC over Bangalore on the day before the sun halo on May 23, 2021, shows a positive enhancement of about 55%. On the sun halo day of May 24, 2021, the rTEC gradually decreased to zero when the halo started at 11:00 UT and started to increase at 12:00 UT when the halo ended, attaining a peak value of about 50% around 16:00 UT. About 17% rTEC was recorded around 18:00 UT on the day after the sun halo on May 25, 2021. Over Cape Town on the day before the sun halo on October 25, 2020, the positive enhancement of rTEC was observed during the morning hour. The significant enhancement of rTEC was observed at 07:30 UT on October 26, 2020. The values of rTEC over North Dakota show opposite trends as compared to Bangalore and Cape Town stations. During the day before the sun halo on December 26, 2021, the positive enhancement of rTEC was observed at about 40% around 22:00 UT.

The scale or time in minutes (0.0625, 0.125, 0.5, 1, 2, 4, 8) of the signal oscillations in each wavelet over the period specified on the X-axis in the time series in hours is represented by the Y-axis in Figure 3. Also Since scale = 1/frequency, the

lower the scale value, the greater the frequency, and vice versa. The cone of influence (the thin black line curve) splits the time-frequency system and demonstrates the validity of the data contained inside the curve. Going off the curve, on the other hand, reduces usefulness. Furthermore, the black-outlined color index intensity appearance indicates the concentration of power at a 95% confidence level or a 5% significance level [35-36]. The colour index represents the intensity of rTEC at each station.

Figure 3 shows the CWT results of the relative change in total electron abundance before, during, and after the solar halo day at each station. Color indices represent the intensity of the power spectrum. This period provides the oscillations in the wavelet corresponding to the significant period from 1 to 4 minutes. Note the sharp increase in rTEC just before the sun's halo begins at 18:00 UT via Bangalore, Cape Town, and North Dakota. It is captured by the wavelet transform as seen in the high-power region of the wavelet spectrum.
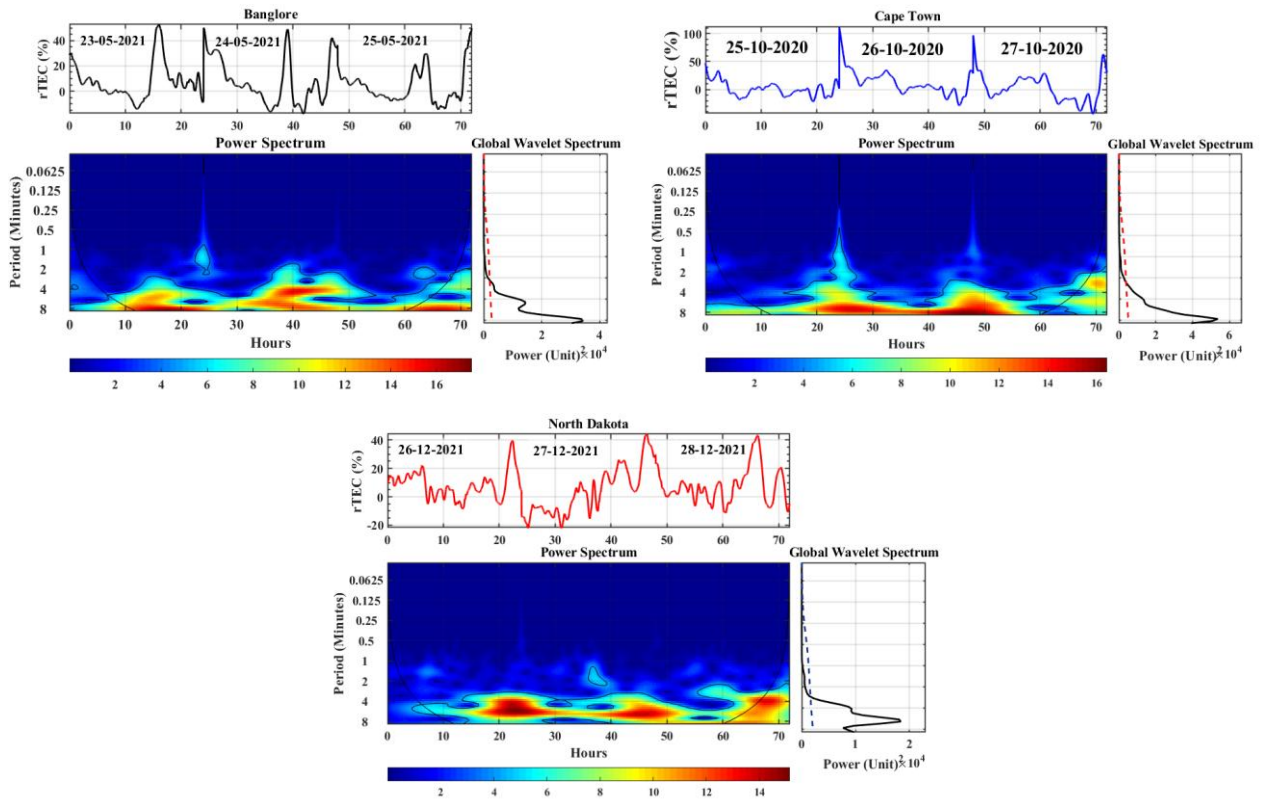
Fig. 3: Variations of relative change in TEC and continuous wavelet transform over Bangalore, Cape Town, and North Dakota during the sun halo day on May 24, 2021, October 26, 2020, and 27, December 2021 respectively.

From Figure 3 over the North Dakota station, a short discontinuous signal is observed in the lower period region. Also, dominant frequencies were observed at lower scales, suggesting that the rTEC exhibits high-frequency behavior at each station. Thus, the fair and consistent performance improvement of WPS marks the most turbulent period that could represent Halo's significant impact on rTEC. In general, stations with larger rTEC have larger power and global wave spectra. Cape Town has a larger rTEC, a larger power spectrum, and a larger global wave spectrum than the Bangalore and North Dakota stations.

3.4. TEC uncertainty over three stations before, during and after sun halo days

Figure 4 shows the relative changes in TEC during the normal days and the sun halo day, and the TEC uncertainty over Bangalore, Cape Town, and North Dakota stations is plotted, respectively. The values of TEC uncertainty were increased to 2.8 TECU before, during, and after the sun halo days over Bangalore station. Before the sun halo day, the value of TEC uncertainty increased to 1.4 TECU at 12:00 UT over Cape Town station. During the time when the sun halo happens at midday, the TEC uncertainty value is about 0.6 TECU over Cape Town. At 22:00 UT on December 27, 2021, the TEC uncertainty of about 1.3

TECU was seen over North Dakota. However, during the day after the halo on December 28, 2021, the TEC uncertainty value was about 1.45 TECU at 18:00 UT. In general, over Cape Town and North Dakota, during the days when a halo occurred and after the halo, the greater values of TEC uncertainty were seen.
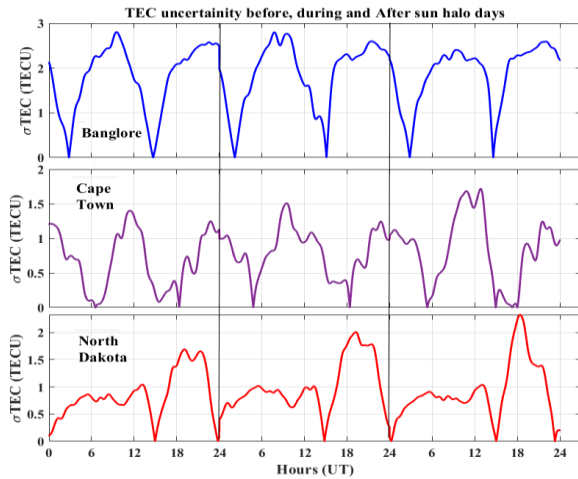
Fig. 4: TEC uncertainties over Bangalore, Cape Town, and North Dakota during the sun halo day on May 24, 2021, October 26, 2020, and 27, December 2021 respectively.

3.5. Variations of solar wind parameters during the sun halo days.

The solar wind is a stream of charged particles (plasma) that the sun emits. This stream's speed, density, and temperature are continually changing [37]. When solar wind leaves a coronal hole, the most dramatic variation in these three parameters occurs [38]. A coronal holes stream can be considered a steady, high-speed stream of solar wind, but a coronal mass ejection is more like a massive, fast-moving cloud of solar plasma. As these solar wind structures reach Earth, they collide with the planet's magnetic field, allowing solar wind particles to enter our atmosphere near our planet's magnetic north and south poles [39]. The solar wind particles interact with the atoms that make up our atmosphere, such as nitrogen and oxygen atoms, releasing energy that is slowly released as light [40-41]. The solar wind is formed by a magnetized and nearly collision-less plasma streaming from the hot solar corona [42-43]. Figure 5 shows solar wind parameters during normal days and the sun halo day over Bangalore, North Dakota, and Cape Town stations.

During the sun's halo day on May 24, 2021, the characteristics of the solar wind parameters were discussed. Before the halo, the Dst index is lower, but it rises throughout and after the halo. During the sun halo, however, the interplanetary magnetic field, IMF Bz, remains southward polarized until 06:00 UT. The solar wind electric field, IEF Ey, and Kp index values are all positive, while the solar activity, as explained by the solar flux (f10.7 cm), is lower during the halo, indicating that the sun is brighter during the halo day, which leads to an increase in ionospheric TEC over Bangalore Station during the halo day than on other days. During the sun halo day over Bangalore on May 24, 2021, the solar wind plasma temperature and proton density are useful in determining the properties of the ionospheric total electron content with solar wind plasma speed. The temperature of solar wind plasma varies before, during, and after sun halo days. However, from the day before the sun halo to the day following the sun halo, it drops from a higher value to a lower one. The plasma speed decreased on May 24, 2021. During the days before and after the sun halo and during the sun halo day, the value of the solar wind proton density steadily increases. During the sun halo day of May 24, 2021, an increase in solar wind proton density may lead to an increase in the relative changes in ionospheric total electron content over Bangalore in the Indian sector.

During the sun halo day on October 26, 2020, the characteristics of the solar wind parameters were also discussed. The Dst index is lower before and during the halo, then rises thereafter. During the sun halo day, however, the interplanetary magnetic field, IMF Bz, remains northward polarized until 06:00 UT. The prompt penetration electric field, IEF Ey, and Kp index values decreased from 00:00 to 04:00 UT and increased from 04:00 to 06:00 UT, and the solar activity explained by the solar flux (f10.7 cm) decreased during the halo, indicating that the sun's activity is brighter during the halo day, leading to an increase in ionospheric TEC over Cape Town station during the halo day than on other days. The values of solar wind plasma temperature, solar wind proton density, and solar wind speed during the sun halo on October 26, 2020, show the same characteristics, and they are also very helpful in showing the characteristics of TEC during the sun halo day. The temperature of the solar wind plasma swings on the day before the sun halo, and it increases higher during the sun halo than on regular days. In addition, the value of solar wind proton density follows the same patterns as the temperature of the solar wind and plasma speed. It

also varies during the day before the sun halo and is higher on sun halo days than on other days. On October 26, 2021, an increase in solar wind proton density during the sun halo day may lead to an increase in relative variations in ionospheric total electron concentration above Cape Town.
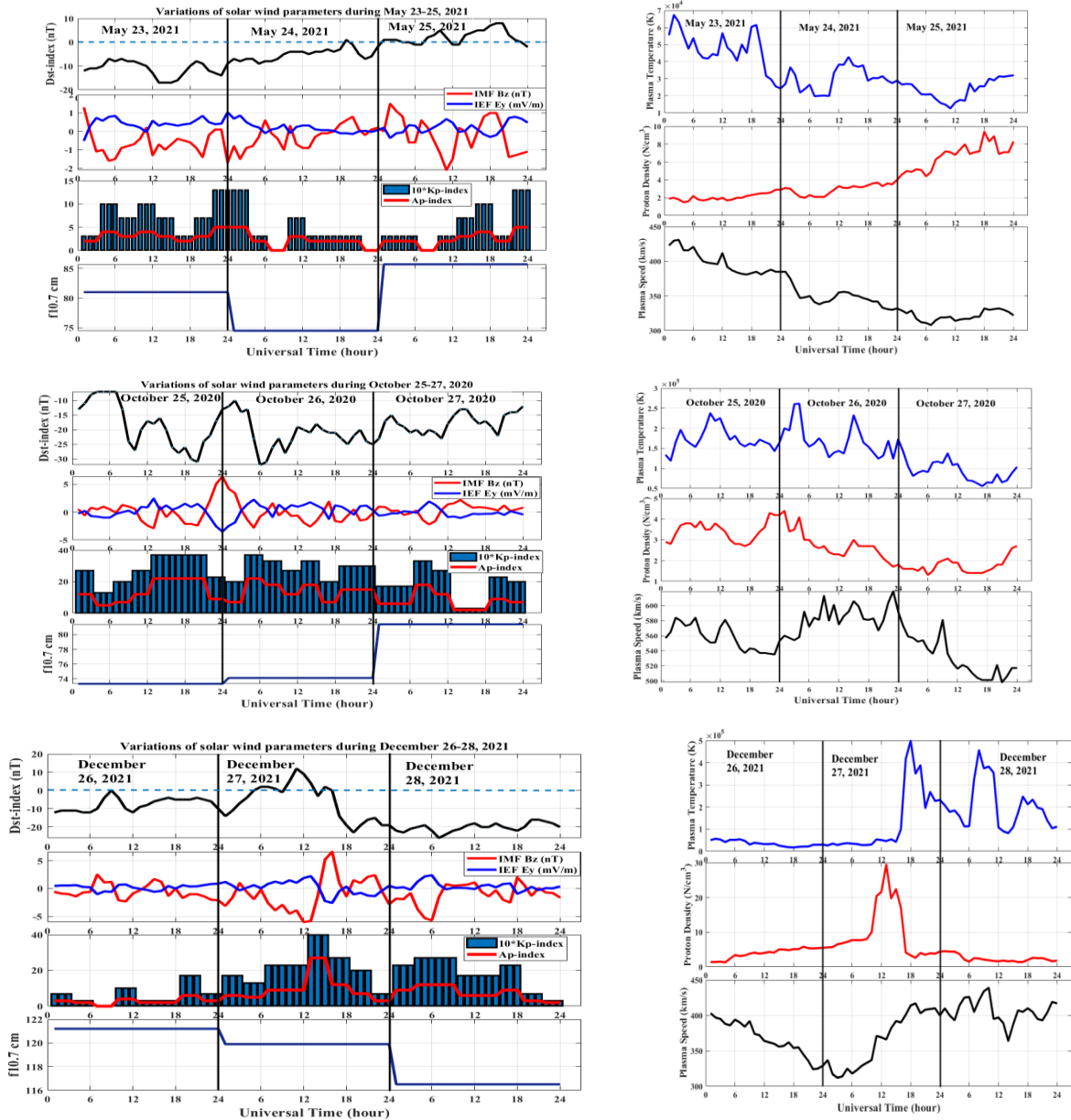
Fig. 5: Variations of solar wind parameters over Bangalore, Cape Town, and North Dakota during the sun halo day on 23-25 May, 2021, 25-27 October, 2021, and 26-28 December, 2021 respectively.

Also, during the sun halo on December 27, 2021, the characteristics of solar wind parameters were discussed. The Dst index rises before and during the sun halo, then drops thereafter. During the sun halo day, however, the interplanetary magnetic field, IMF Bz, remains southward polarized until 07:00 UT. Around 07:00 UT, the prompt penetration electric field, IEF Ey, and Kp index values increased, while the solar activity explained

by the solar flux (f10.7 cm) decreased after the halo, indicating that the sun's activity is less intense during the sun halo day than the day following the sun halo day. The parameters of solar wind plasma temperature and proton density are also highly useful in displaying the characteristics of ionospheric TEC on December 27, 2021, during the sun halo day above North Dakota. Solar wind plasma temperature values range from less than one

during the day before the sun halo to about 13:00 UT during the sun halo days and rise from roughly 13:00 UT on the day of the sun halo until the day following the sun halo day. The solar wind speed also increased from 06:00 UT to 18:00 UT on December 27, 2021. In addition, the value of solar wind proton density follows the same patterns as the temperature of the solar wind and plasma speed. It also displays typical values ranging from less than one the day before the sun halo to about 13:00 UT on the days when the sun halo is visible. However, it rises from roughly 13:00 UT on the day of the sun halo day until the day following the sun halo day. The increase in solar wind proton density with solar wind speed from 13:00 UT on sun halo day to a day after the sun halo day leads to an increase in relative changes in ionospheric total electron content over North Dakota in American states and a decrease in TEC on December 27, 2021, during the sun halo day. The parameters of solar wind plasma temperature and proton density are also highly useful in displaying the characteristics of ionospheric TEC on December 27, 2021, during the sun halo day above North Dakota.

4. CONCLUSIONS

This study examines the responses of TEC to solar flares during the three sun halo days on three GPS stations in low and middle latitude regions using ionospheric parameters. The key results of the study are discussed as follows:

❖ TEC patterns are similar over Bangalore and Cape Town stations throughout the solar halo day, whereas opposing trends are seen over North Dakota. The values of TEC at low-latitude stations (Bangalore) and mid-latitude stations (Cape Town and North Dakota) were compared. Greater values of TEC were observed over low-latitude stations (Bangalore) than over mid-latitude stations (Cape Town and North Dakota) during the days before, during, and after the sun halo days. The disturbance dynamo electric field and prompt penetration electric field effects associated with disturbed geomagnetic conditions are more likely to cause TEC enhancement at low-latitude stations than at mid-latitude stations [44-45].

❖ Positive relative change in TEC dominates during the sun's halo over Bangalore and Cape Town stations. Stations that have greater rTEC have a greater power spectrum and global wave spectrum. Cape Town has a greater rTEC and a greater power spectrum and global wave spectrum than Bangalore and North Dakota stations.

❖ On May 24, 2021, about 320 km/s solar wind speed and 4.9 protons/cm^3, 1.3 Kp-index and 5 Ap-index values with x-ray solar flares for about 6 hours, having the maximum B1.47 and B4.8 classes at 19:00 UT and 00:34 UT, were observed. This may be the probable cause for TEC value to be enhanced during the sun halo day on May 24, 2021, rather than during the days before and after sun halo days over Bangalore station. On October 26, 2020, about 557.9 km/s solar wind speed and 45.9 protons/cm^3, 3.8 Kp-index and 21 Ap-index values with x-ray solar flares for about 6-hours having the maximum B1.85 and B2.31 classes at 23:36 UT and 17:01 UT were observed. This may be the probable cause for TEC value to be enhanced during the sun halo day on October 26, 2020, rather than during the days before and after sun halo days over Cape Town station. On December 27, 2021, about 432 km/s solar wind speed and 4.6 protons/cm3, 4 Kp-index and 22 Ap-index values with x-ray solar flares for about 6 hours having the maximum C2.27-classes at 23:35 UT were observed. This may be the probable cause for TEC value to be enhanced during the sun halo day on December 27, 2021, rather than during the days before and after sun halo days over North Dakota station.

Finally, in this study, we have seen that the effects of solar flares that occurred during the three sun halo days with the presence of solar wind speed, solar wind proton density, a f10.7 value greater than 74 sfu, and cloud plasmas emitted by the sun with negative values of Dst-index and IMF Bz are the main causes for the enhancement of TEC over three stations. However, during the time gap between when the sun halo begins and ends the values of changes in TEC and rTEC shows a negative response. In general, solar flares have a major influence on ionosphere electrodynamics, and the upward ExB drifts increase over a longer period of time, inducing TEC disturbances [46].

This is the first study conducted on the responses of ionospheric TEC to solar flares during the sun halo days over low and mid-latitude regions. Therefore, the authors of this work recommend that the relationship between solar flares and sun halos with their effects on TEC over the ionospheric regions needs further study in future work.

REFERENCES

[1] Robert, V. R. and Chunyan, L. Atmospheric optical effects in the coastal zone. In *Meteorology for Coastal Scientists*, pages 469–483. Springer (2021).

[2] David, K. L., William, C. L., and William, L. *Color and light in nature*. Cambridge University Press (2001).

[3] Emilia, P. Prehistoric light in the air. *The Oxford Handbook of Light in Archaeology*, page 355 (2021).

[4] David, K. L. Atmospheric halos. *Scientific American*, **238** (4): 144–153 (1978).

[5] Tony, B. Colors in earthâ€™s atmosphere. In *The Rainbow Sky*, pages 195–265. Springer (2010).

[6] Sung, M. H. and Gladimir, B. A study on atmospheric halo visualization, 2003 (2003).

[7] Marinus Anthony van der Sluijs-Seongnam and Peter James-London. Saturn as the â€œsun of nightâ€• in ancient near eastern tradition. *Aula Orientalis*, **279** (321): 0212–5730 (2013).

[8] Yngvar, G. and Carl, S. B. The effect of suspended ice crystals on radiative cooling. *Journal of Applied Meteorology (1962-1982)*, pages 446–453 (1965).

[9] Moldwin, M. An introduction to space weather. Cambridge University Press (2022).

[10] Stanimir, M. S.; Nicolas, B.; David, B., David, B.; Carine, B. et al. Multi-instrument observations of the solar eclipse on 20 march 2015 and its effects on the ionosphere over belgium and europe. *Journal of Space Weather and Space Climate*, **7**: A19 (2017).

[11] Xiaohua, F.; David, P.; Yingjuan, M.; Stephen, B.; Edward, T. et al. Mars upper atmospheric responses to the 10 september 2017 solar flare: A global, time-dependent simulation. *Geophysical research letters*, **46** (16): 9334–9343 (2019).

[12] Joseph, W. C. and Donald, M. H. *Theory of planetary atmospheres: an introduction to their physics and chemistry*. Academic Press (1990).

[13] Rainer, S. Space weather: The solar perspective. *Living reviews in solar physics*, **3** (1): 1–72 (2006).

[14] César, B. A. O.; Teddy Modesto Surco Espejo, Alison Moraes, Emanoel Costa, Jonas Sousasantos, Luis, F. D. L. and Mangalathayil, A. A. Analysis of plasma bubble signatures in total electron content maps of the low-latitude ionosphere: A simplified methodology. *Surveys in geophysics*, **41** (4): 897–931 (2020).

[15] Leonard, K.; Daniel, M.; Eleri, P. S.; Ljiljana, R. C.; Ruth, A. B. et al. Total electron content-a key parameterin propagation: measurement and usein ionospheric imaging. *Annals of Geophysics*, **47** (2-3 Sup.): … (2004).

[16] Liying, Q.; Alan, G. B.; Stanley, C. S. and Phillip, C. C. Solar flare impacts on ionospheric electrodyamics. *Geophysical research letters*, **39** (6): … 2012.

[17] Edward, L. A.; Elvira, I. A.; Vladislav, V. D.; Ilya, K. E.; Nadezhda, S. G.; Artem, B. I.; Eugene, A. K.; Lyudmila, A. L.; Oleg, S. L.; Kirill, S. P. et al. A review of gps/glonass studies of the ionospheric response to natural and anthropogenic processes and phenomena. *Journal of Space Weather and Space Climate*, **3**: A27 (2013).

[18] Daniela, W.; Jens, B. and Norbert, J. Space weather activities in germany (2017).

[19] Singh, A.; Rao, S. S.; Rathore, V. S.; Singh, S. K. and Singh, A. K. Effect of intense solar flares on tec variation at low-latitude station varanasi. *Journal of Astrophysics and Astronomy*, **41** (1): 1–14 (2020).

[20] Hussein, M. F.; Ramy, M.; Essam, G. and Akimasa, Y. The impact of coronal mass ejections on the seasonal variation of the ionospheric critical frequency f0 f2. *Universe*, **6** (11): 200 (2020).

[21] Kanaka, D. R.; Panda, S. K.; Sharma, S. K.; Singh, A. K.; Kurnala, K.; Haritha, C. S. and Wuyyuru, S. Anomaly effects of 6–10 september 2017 solar flares on ionospheric total electron content over saudi arabian low latitudes. *Acta Astronautica*, **177**: 332–340 (2020).

[22] Chakraborty, M.; Singh, A. K. and Rao, S. S. Solar flares and geomagnetic storms of september 2017: Their impacts on the tec over 75 e longitude sector. *Advances in Space Research*, **68** (4): 1825–1835 (2021).

[23] Uga, C. I.. Effects of geomagnetic storm on ionospheric tec variability over high latitude regions. *Astrophysics and Space Science*, **10** (2): 18–27 (2022).

[24] Idosa, C. and Shogile, K. Variations of ionospheric tec due to coronal mass ejections and geomagnetic storm over new zealand. *New Astronomy*, **99**: 101961 (2023).

[25] Idosa, C. U. and Rikitu, K. S. Effects of total solar eclipse on ionospheric total electron content over antarctica on 2021 december 4. *The Astrophysical Journal,* **932** (1): 2 (2022).

[26] Tang, W.; Jin, L. and Xu, K. Performance analysis of ionosphere monitoring with beidou

cors observational data. *The Journal of Navigation*, **67** (3): 511–522 (2014).

[27] Hernández-Pajares, M.; Juan, J. M.; Sanz, J.; Aragón-Àngel, À.; Garcá-Rigo, A. et al. The ionosphere: effects, gps modeling and the benefits for space geodetic techniques. *Journal of Geodesy*, **85** (12): 887–907 (2011).

[28] Seemala, G. K. and Valladares, C. E. Statistics of total electron content depletions observed over the south american continent for the year 2008. *Radio Science*, **46** (05): 1–14 (2011).

[29] Ansari, K.; Corumluoglu, O. and Panda, S. K. Analysis of ionospheric tec from gnss observables over the turkish region and predictability of iri and spim models. *Astrophysics and Space Science*, **362** (4): 1–24 (2017).

[30] Adhikari, B.; Baruwal, P. and Chapagain, N. P. Analysis of supersubstorm events with reference to polar cap potential and polar cap index. *Earth and Space Science*, **4** (1): 2–15 (2017).

[31] Adhikari, B. and Chapagain, N. P. Polar cap potential and merging electric field during high intensity long duration continuous auroral activity. *Journal of Nepal Physical Society*, **3** (1): 6–17 (2015).

[32] Adhikari, P. B.; Adhikari, A. and Adhikari, B. Application of the wavelet transform on the unusual lightning flashes of the himalayan region, nepal. *The Scientific World Journal*, *2022* (2022).

[33] Khanal, K.; Adhikari, B. Chapagain, N. P. and Bhattarai, B. Hildcaa-related gic and possible corrosion hazard in underground pipelines: A comparison based on wavelet transform. *Space Weather*, **17** (2): 238–251 (2019).

[34] Markovic, D. and Koch, M. Wavelet and scaling analysis of monthly precipitation extremes in germany in the 20th century: Interannual to interdecadal oscillations and the north atlantic oscillation influence. *Water Resources Research*, **41** (9): … (2005).

[35] Manyilizu, M.; Dufois, F.; Penven, P. and Reason, C. Interannual variability of sea surface temperature and circulation in the tropical western indian ocean. *African Journal of Marine Science*, **36** (2): 233–252 (2014).

[36] Shi, B.; Yang, X. and Yan, L. Optimization of a crude distillation unit using a combination of wavelet neural network and line-up competition algorithm. *Chinese Journal of Chemical Engineering*, **25** (8): 1013–1021 (2017).

[37] Gosling, J. T. The solar wind. In Encyclopedia of the solar system, pages 261-279. Elsevier (2014).

[38] Cranmer, S. R.; Gibson, S. E. and Riley, P. Origins of the ambient solar wind: implications for space weather. *Space Science Reviews*, **212** (3): 1345–1384 (2017).

[39] Jain, K. and Komm, R. W. Asian journal of physics. *Asian Journal of Physics*, **25** (3): 363–386 (2016).

[40] Johnstone, C. P. The influences of stellar activity on planetary atmospheres. *Proceedings of the International Astronomical Union*, **12** (S328): 168–179 (2016).

[41] Singh, A. K.; Bhargawa, A.; Singh, D. and Singh, R. P. Physics of space weather phenomena: A review. *Geosciences*, **11** (7): 286 (2021).

[42] Gosling, J. T. The solar wind. In *Encyclopedia of the solar system*, pages 261–279. Elsevier (2014).

[43] Heidrich-Meisner, V. and Wimmer-Schweingruber, R. F. Solar wind classification via k-means clustering algorithm. In *Machine learning techniques for space weather*, pages 397–424. Elsevier (2018).

[44] Polekh, N.; Zolotukhina, N.; Kurkin, V.; Zherebtsov, G.; Shi, J. et al. Dynamics of ionospheric disturbances during the 17–19 March 2015 geomagnetic storm over East Asia. *Advances in Space Research*, **60** (11): 2464-2476 (2017).

[45] Singh, R.; Lee, Y. S.; Song, S. M.; Kim, Y. H.; Yun, J. Y. et al. Ionospheric Density Oscillations Associated With Recurrent Prompt Penetration Electric Fields During the Space Weather Event of 4 November 2021 Over the East-Asian Sector. Journal of Geophysical Research: *Space Physics*, **127** (6): e2022JA030456 (2022).

[46] Qian, L.; Burns, A. G.; Solomon, S. C. and Chamberlin, P. C.. Solar flare impacts on ionospheric electrodyamics. *Geophysical research letters*, **39** (6): … (2012).